Ligand Radical Mediated Water Oxidation by a Family of Copper o -Phenylene Bis-oxamidate Complexes

Samir Chattopadhyay, Arnab Ghatak, Youngju Ro, Régis Guillot, Zakaria Halime, Ally Aukauloo, Abhishek Dey

Ligand Radical Mediated Water Oxidation by a Family of Copper o-Phenylene Bis-Oxamidate Complexes

Samir Chattopadhyay,[a] Arnab Ghatak,[a] Youngju Ro,[b] Régis Guillot,[b] Zakaria Halime [b] Ally Aukauloo[b,c] and Abhishek Dey[a]**

a) School of Chemical Sciences, Indian Association for the Cultivation of Science, Jadavpur, Kolkata-700032, India.

b) Université Paris Sud, CNRS, F-91405 Orsay Cedex, France.

c) Institute for integrative Biology of the Cell (I2BC), CEA, CNRS Université Paris-Saclay, UMR 9198, F-91191, Gif-sur-Yvette, France.

KEYWORDS (Word Style "BG_Keywords")

ABSTRACT

Understanding the reactivity landscape for the activation of water till the formation of the O-O bond and O_2 release in molecular chemistry is a decisive step in guiding the elaboration of cost-effective catalysts for the oxygen-evolving reaction (OER). Copper (II) complexes have recently caught the attention of chemists as catalysts for the $4e^-/4H^+$ water oxidation process. While a copper (IV) intermediate has been proposed as the reactive intermediate species, yet no spectroscopic signature has been reported so far. Copper (III) ligand radical species have also been formulated and supported by theoretical studies. We found, herein, that the reactivity sequence for the water oxidation with a family of Copper (II) o-phenylene bisoxamidate complexes are a function of the substitution pattern on the periphery of the aromatic ring. In-situ IR, EPR and rR spectroelectrochemical studies helped to sequence the elementary electrochemical and chemical events leading towards the O_2 formation selectively at the copper center. A copper (II) superoxide species is identified as the reactive intermediate, the stability of which governs the selectivity of $4e^-$ oxidation of water to molecular oxygen.

INTRODUCTION

Water oxidation reaction (WOR) is indisputably one of the main hurdles in developing sustainable ways to store solar energy.[1-4] This half-reaction provides the electrons and protons for further synthesis of H_2 or reduction of CO_2 in energy-rich compounds.[5-7] In nature, a Mn_4CaO_5 cluster, known as the Oxygen Evolving Complex (OEC), located at the heart of Photosystem II, is the locus where this reaction takes place.[8-16] Close structural mimics of the OEC have been achieved however their catalytic reactivities have not met our expectations yet.[17-18] Both the advancement on the functioning of this enzyme and effort of chemists to develop

robust catalysts are bringing this target closer to reality.[13, 19-21] Although much success has been achieved with ruthenium and iridium complexes in this quest, there is still an urgent need to elaborate cost-efficient catalysts based on more abundant metal.[22-27] On the contrary, significant progress in catalytic water oxidation has been made with iron, cobalt, and manganese complexes in the homogeneous medium either by the addition of chemical oxidants such as cerium (IV) or ruthenium (III) salts or under electrochemical conditions.[28-34] Recently, copper complexes have joined the short list of molecular catalysts for the WOR.[35-43] Reasons behind this stem from the copper oxygenase functions where O_2 activation leads to the cleavage of the O-O bond leading to highly oxidized copper species.[44] Hence reversing the activation steps from H_2O to form O-O bond is an attractive perspective. Mayer and co-workers, first exemplified such strategy in the electrocatalytic OER with a dinuclear bipyridine Cu^{II}-di-μ-hydroxo complex.[35] While Meyer and coworkers discovered that single site copper complexes with the particularity of having deprotonated amido functions in the coordination sphere were effective electrocatalysts for O_2 release. Mechanistically, a Cu(III) intermediate was predicted. However, no clear spectroscopic signature has yet been unraveled for the formal Cu(IV) active catalytic species.[36] An alternate electronic structure proposed for this intermediate is a Cu(III)-ligand radical species.[19, 45] More recently, Llobet and co-workers have reported on the electrocatalytic water oxidation with a copper (II) bis-oxamidate complex.[46-47] Here too, a Cu(III)-ligand radical species has been invoked in the O-O bond formation. The authors put forward an original mechanism for the O-O bond formation tagged as SET-WNA (Single Electron Transfer - Water Nucleophilic Attack), where no direct Cu-O intermediate pertains during the catalytic cycle.[46] Such a proposal has caught our attention as we have been interested to use electrochemical techniques coupled to IR, EPR and rR spectroscopy to gain insights into the mechanistic routes for the O_2 formation.

Polyanionic chelating ligands were found to stabilize the unusual copper(III) oxidation state as evidenced with o-phenylene-bis amidate ligands.[48-49] Further studies also evidenced that these families of ligands could be the siege for competitive ligand *vs.* metal-centered redox behavior depending on the substitution pattern on the aromatic ring.[50-51] The recent findings that in the basic medium the single site copper(II) bisoxamidate (OPBI) complexes were potential candidates for the WOR have prompted us to interrogate the electronic properties of the activated forms. In this report, the electrocatalytic behavior of three substituted N,N'-orthophenylene-bis(N-methyloxamidate) copper(II) complexes (Fig. 1) towards water oxidation under both homogeneous and heterogeneous conditions was studied along with their spectroelectrochemical investigations. It was found that the overpotential for the WOR is a function of the electron donating and withdrawing ability of the substituents present on the phenylene ring as observed previously by Llobet and coworkers. In-situ IR and EPR spectroscopy evidenced that both oxidation processes from the starting Cu (II) derivative are ligand centered under the operating conditions providing an alternate formulation of the active species responsible for the OER in the catalytic cycle. The binding of the OH^- to the metal center occurs either after the first or second oxidation process depending on the nature of the substituents on the central aromatic fragment. A ligand based monoradical bound Cu^{II}-O_2^- is identified as the reactive intermediate species under catalytic conditions using rR spectroelectrochemical technique and the stability of which is responsible for the $4e^-/4H^+$ oxidation of H_2O to O_2.

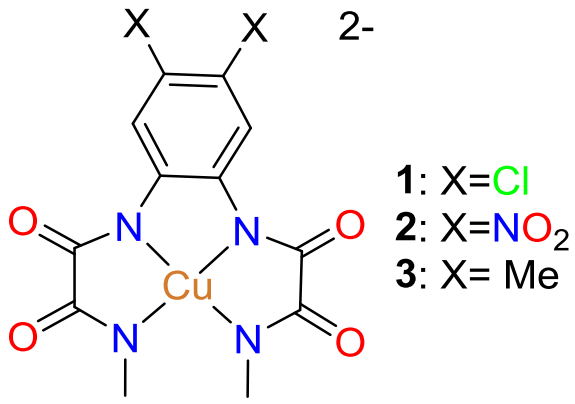

Figure 1: Chemical structure of the compounds used in the present study where compounds **1**, **2** and **3** contains -Cl, -NO_2 and -Me, respectively, in the position of X in the structure. The complex is stabilized by PPh_4^+ counter cations.

RESULTS AND DISCUSSION

Cyclic voltammetry (CV) of the compounds was done in acetonitrile having 1 mM of the catalysts in the presence of 100 mM tetra butyl ammonium perchlorate (TBAP) as supporting electrolyte (Fig. 2). All of the three compounds exhibit three redox processes which are a function of the electron-donating and withdrawing nature of the -X substituents. In the case of compound **1**, two reversible redox processes are observed at 0.13 V, 0.65 V along with a quasi-reversible process at 1.28 V. In the case of **2**, all of these redox processes are shifted to more anodic potentials as the presence of strong withdrawing group, -NO_2, makes the complex harder to oxidize.[52] While a cathodic shift was observed with electron-donating methyl (-Me) substituent in complex **3**. The cyclic voltammogram of **3** shows the same faradaic response as observed previously by Llobet and coworkers.[46]

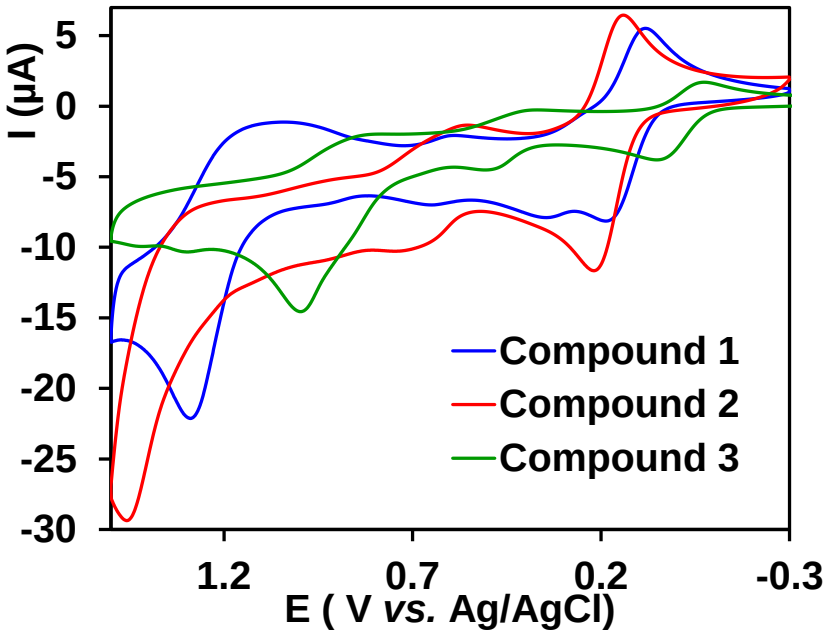

Figure 2: Cyclic voltammograms of the compounds (1 mM) in acetonitrile containing 100 mM TBAP as electrolyte. Here, Glassy carbon (GC), platinum and a sealed aqueous Ag/AgCl (saturated KCl) were used as working, counter and reference electrode, respectively.

(I)EPR spectroelectrochemistry under non-catalytic conditions:

EPR spectroelectrochemistry was performed to describe the locus of the oxidation processes under our experimental conditions. Upon holding the potential (at 0.9V) above the first oxidation process, the EPR spectra of **1**, **2** and **3** show (Fig. 3 A, C, and E, red line, Fig. S15) the presence of both Cu(II) and a ligand-based radical, such that one electron oxidized form can be best formulated as a $[Cu^{2+}L^{3-}]$ state (Cu(II)-ligand monoradical). The observation of both Cu(II) and ligand radical signals is indicative of lack of coupling between the spin on the $d_{x^2-y^2}$ orbital on Cu on the equatorial plane and the spin on the π orbitals of the ligand which is perpendicular to the equatorial plane as is observed for several square planar Cu complexes with non-innocent ligands.[52-56] Previously, on a related system, density functional theory calculations suggests that the Cu(II)-ligand monoradical is ~ 20 kcal/mol more stabilized relative to the corresponding

Cu(III) species when the parent complex undergoes single electron oxidation.[52] Interestingly, the intensity of the radical signal decreases upon electrolysis after the second oxidation wave at 1.2 V while the signals of Cu^{2+} are maintained intact (Fig. 3 A, C, E green, Fig. S15). The loss of intensity of the radical signal reflects the formation of a ligand-based diradical species [$Cu^{2+}L^{2-}$] from the Cu (II)-ligand monoradical species, where the two radicals are anti-ferromagnetically coupled to each other.[52] The coupling between two ligand radicals in the π plane is mediated by the filled $d_{zx/yz}$ orbitals of the Cu^{2+} center.[57-58] Further fine analysis of the EPR hyperfine constant yields the ligand field parameters and covalency of the Cu^{2+} center (β^2 in eq. 1)[59-61]

$$A_P = Pd\left[-\kappa\beta^2 - 0.57\beta^2 + (g_P - 2.0023) + 0.43(g_\perp - 2.0023)\right] \quad \text{.....(1)}$$

Where A_P, g_P and g_P are experimentally determined (Table S3, Fig. S15), Pd and κ are constants, the value of which are: Pd[Cu^{2+}] =400×$10^{-4}$$cm^{-1}$ and κ[Cu^{2+}] =0.43.

The β^2 values report the changes in the chemical environment around the Cu^{2+} ion (Table S3) in the monoradical and diradical states. The increase in β^2 values of the Cu (II) center (Table S3) in **1** and **3** upon successive oxidations (0.9 V and 1.2 V) is a clear indication of the fact that the tetradentate ligand undergoes oxidation making it a weaker donor. However, the environment around the metal center is unaltered upon the second oxidation which is better represented in the difference spectra between the EPR data obtained after the first and the second oxidation (Fig. 3 B, D, F blue and red lines) where the signal from the Cu(II) center cancels off for both **1** and **3** indicating that the Cu(II) center is not sufficiently perturbed during the second oxidation (Fig. 3(A, B, and E, F) and Table S3). In contrast, **2** shows a shift of β^2(Cu^{2+}) value from 0.67 in the resting Cu (II) state to 0.64 in the ligand monoradical state (Table S3) indicating that it likely forms solvent bound monoradical upon electrochemical oxidation at 0.9V (Fig. 3 C and D).

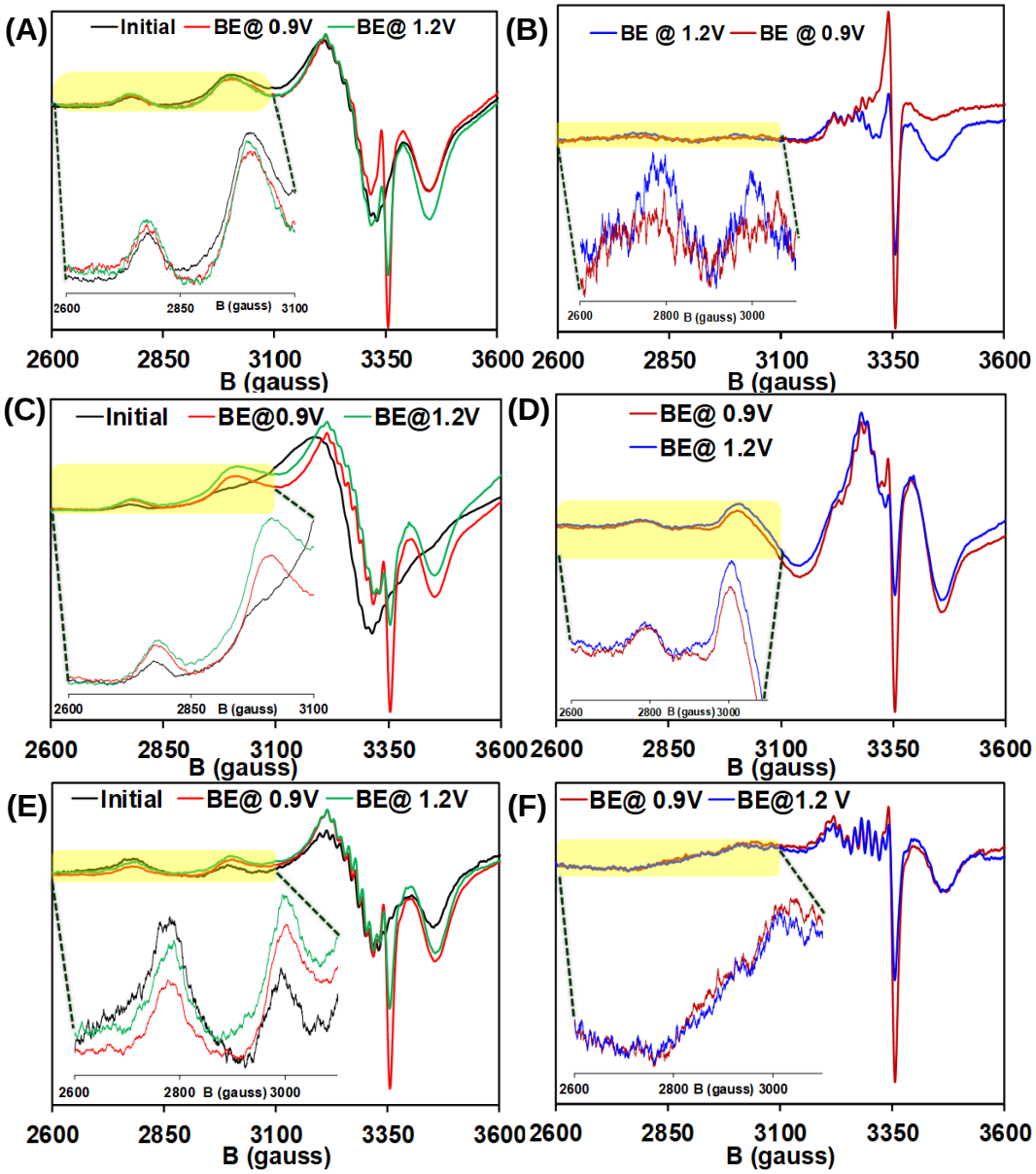

Figure 3: EPR spectra of compounds **1** (A)**, 2**(C) and **3** (E) (1 mM) in acetonitrile having 100 mM TBAP (black-initial, red- after control potential electrolysis at 0.9V and green- after control potential electrolysis at 1.2V). B, D and F are the EPR difference spectra (difference of the samples after respective oxidations from the initial without bulk electrolysis) of **1**, **2**, and **3** respectively.

(II) FTIR Spectroelectrochemistry under non-catalytic conditions:

FTIR spectroelectrochemistry is employed to characterize the successive oxidation products by utilizing the advantage of the intense IR amide chromophores in the ligand backbone. Oxidation of complex **1** at 0.9 V results in a shift of the amide vibrations from 1597 and 1618 cm^{-1} to 1667 and 1713 cm^{-1} respectively (Fig. 4A, green and 4B, orange) confirming oxidation of the ligand during the process. Further oxidation at 1.2 V shifts the amide vibration further higher to 1667 and 1738 cm^{-1} (Fig. 4B, sky) consistent with another sequential oxidation of the ligand. The same trend is observed for complex **2** and **3** upon successive oxidations. In the case of **2**, the amide vibrations were observed at slightly higher wavenumbers than **1** (probably due to the presence of electron withdrawing nature of the $-NO_2$ substituents), 1599 and 1626 cm^{-1} (Fig. 4A, red) which increases to 1673 and 1713 cm^{-1} in the monoradical (4C, orange) and to 1713 and 1773 cm^{-1} in the diradical species. (Fig. 4C, sky) In the case of **3**, the amide vibration was detected at 1588 and 1611 cm^{-1} (Fig. 4A, blue) and after the successive oxidations, the corresponding vibration was observed at 1663 and 1713 cm^{-1} in the monoradical species (Fig. 4D, orange) and 1663 and 1736 cm^{-1} in the diradical species. (Fig. 4D, sky) Overall, these data indicate that under non-catalytic conditions, sequential oxidations of the resting Cu (II) species leads to a Cu^{2+}-ligand monoradical (at 0.9 V) and a Cu^{2+}-ligand diradical species (at 1.2 V), consistent with conclusions we obtained from the EPR data.

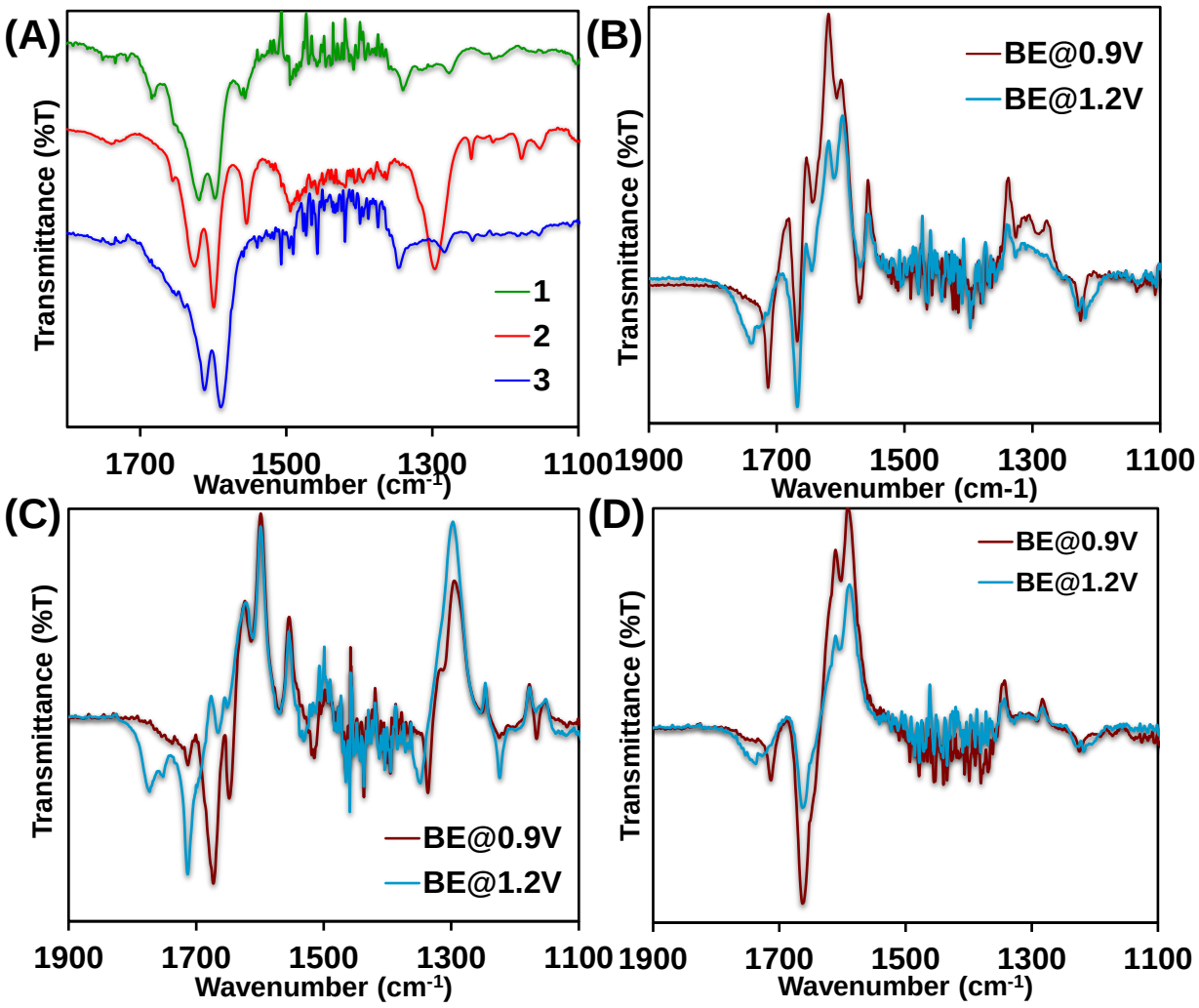

Figure 4: (A) FTIR spectra of the compounds (4 mM in acetonitrile having 100 mM TBAP electrolyte) used in the present study, FTIR spectrochemical data (difference spectra- difference from the initial in acetonitrile without oxidation) of (B) **1**, (C) **2** and (D) **3** upon successive oxidations at 0.9V and 1.2V.

(III) Electrocatalytic oxygen evolution under homogeneous conditions:

The catalytic oxygen evolution by compound **1** was investigated in acetonitrile by adding different amounts of an organic base (tetra butyl ammonium hydroxide, TBAH). A sharp increase in the current was observed replacing the irreversible response at 1.2 V (Fig 5A). This

electrocatalytic process is pseudo 1st order with respect to both catalyst and the substrate (here, TBAH) (Fig. S3). The linear variation of catalytic peak current with the concentration of catalyst also pertains a single site mechanism of molecular catalysis during oxygen evolution reaction. The k_{cat} was calculated as 3.49 s^{-1} at 50 mVps scan rate at 7 mM TBAH concentration with the help of equation 2.[31, 35] The diffusion coefficient of the catalysts was determined as reported in the SI (Fig. S2).

$$i_c = n_c FAC_{cat}(D_{cat}k_{cat})^{1/2} \quad \text{.....(2)}$$

Where, i_c, and n_c are the maximum catalytic current and number of electron transfer in the catalytic event respectively. The rest terms were discussed in SI. Rinse test was performed to discard the probability of retaining the catalyst at the GC electrode. (Fig. S4). The evolution of O_2 was detected in-situ by reverse cathodic scans where the O_2 produced by the catalyst during anodic scans in an anaerobic solution is reduced (Fig. S5). The Faradaic yield is determined to be 84% by collecting the O_2 gas evolved in an inverted burette set up during bulk electrolysis at 1.2V in 1mM solution of compound **1** in acetonitrile containing 7 mM of TBAH. Bubble formation due to evolution of O_2 is observed on the working electrode during the control potential electrolysis (Fig. S6) The evolution of O_2 has been further confirmed by gas chromatography (GC-TCD) (Fig. S7).

A similar electrochemical reactivity pattern was evidenced with **2** (Table 1, Fig. S8, Fig. S9 and Fig.4 (B)) albeit at higher anodic potential because of the electron withdrawing nature of $-NO_2$. The potential at which the catalytic OER observed for **3** is around 0.98 V which is ~0.2 V lower than that of **1** with a calculated k_{cat} of. 21.4 s^{-1} (Table 1, Fig. 4 (C), Fig. S10 and S11). These noticeable differences in the electrocatalytic activities of **1**, **2** and **3** were provide strong motivations to enquire about the mechanistic facets for this family of complexes. The first

interrogation was whether oxygen formation would borrow an intermediate two-electron oxidation pathway i.e. through H_2O_2 formation. Using the Xylenol orange assay we found that the amount of H_2O_2 formed during oxygen evolution reaction was negligible (<1% H_2O_2) thereby favoring the selective $4e^-$ oxidation of water to molecular oxygen (Fig. S12).

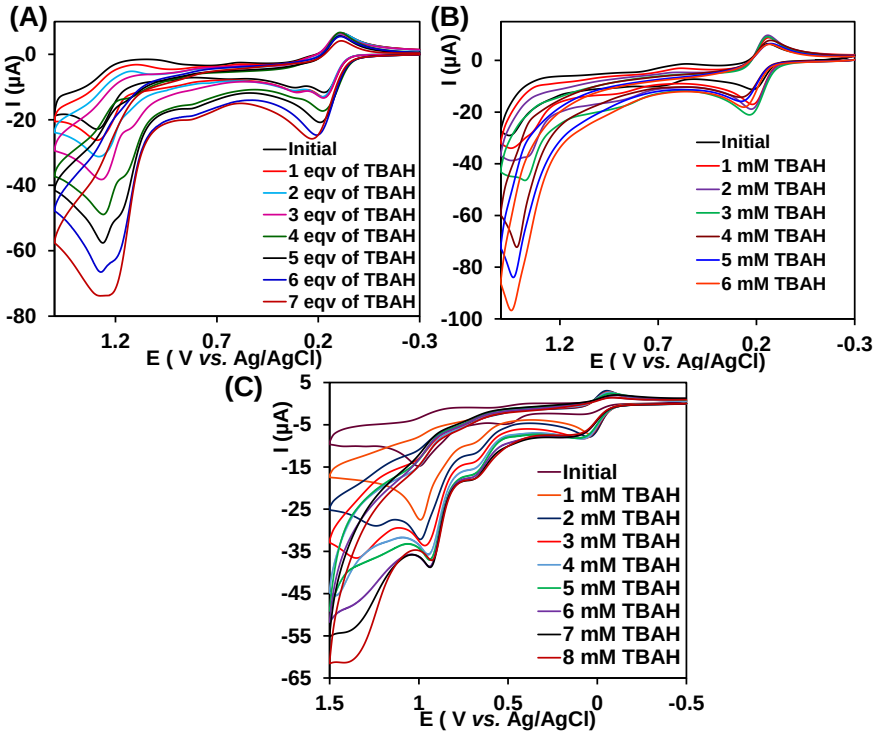

Figure 5: Cyclic voltammograms of (A) **1**, (B) **2**, and (C) **3** (1 mM in acetonitrile containing 100 mM TBAP as electrolyte) showing the homogeneous catalytic oxygen evolution with increasing amounts of TBAH. Glassy carbon (GC), platinum and a sealed aqueous Ag/AgCl (saturated KCl) are used as working, counter and reference electrode, respectively.

(IV) Electrocatalytic water oxidation under heterogeneous conditions:

Compounds **1** and **3** being insoluble in water (due to the presence of PPh_4^+ counter cations) allowed us to perform the oxygen evolution catalysis in an aqueous medium under heterogeneous conditions. This was achieved by drop-casting the catalysts on an EPG electrode. In the linear sweep voltammograms (LSV) in a pH 7 phosphate buffer solution, **3** presented a

remarkable OER catalysis at a very low overpotential of 0.17 V. In contrast, **1** showed only a feeble electrocatalytic current at 0.63 V overpotential under the same conditions (Fig. 6A). Rotating ring disc electrochemistry (RRDE) was performed to verify the production of H_2O_2 ($2e^-$ oxidation) during the oxidation of water to O_2 (Fig. S13). Here too, only 1% of H_2O_2 was detected consistent with the results obtained in homogeneous electrochemical experiments (organic solvents). The LSV of **1** in pH 11 phosphate buffer shows electrocatalytic wave at an overpotential of 0.48 V which drops down to 0.23 V for **3** (Fig. 5 B).

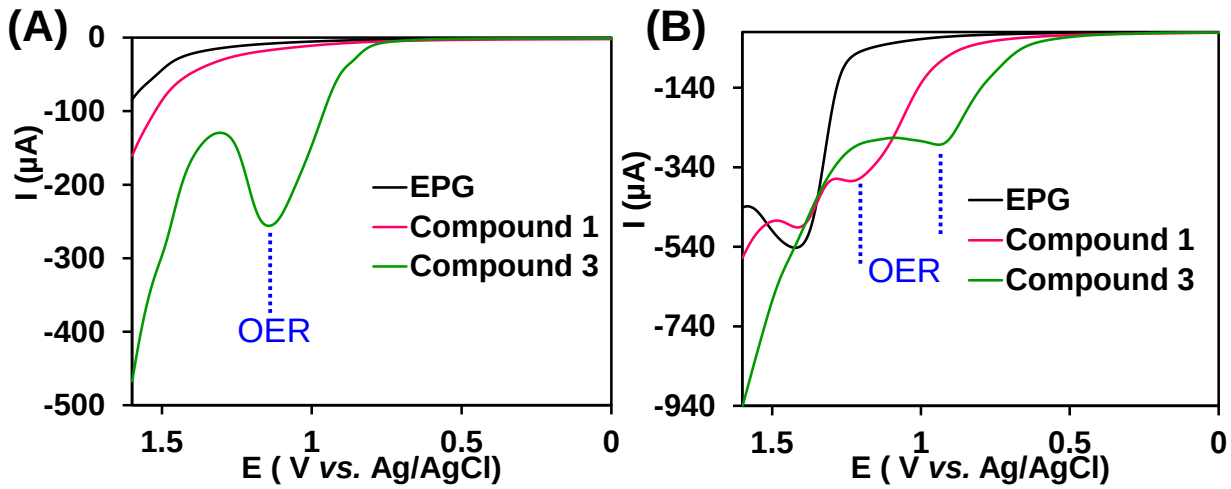

Figure 6: Linear sweep voltammograms of **1** and **3** in (A) pH 7 and (B) pH 11 phosphate buffers (containing 100 mM KPF_6 as supporting electrolyte) showing heterogeneous oxygen evolution reaction by drop-casting the catalysts on top of EPG electrode. Here, EPG, platinum and a sealed aq. Ag/AgCl (saturated KCl) are used as working, counter and reference electrode, respectively.

(V) EPR spectroelectrochemistry under catalytic conditions:

With the central goal to capture the electronic signatures of the reactive intermediates formed under our homogeneous experimental conditions and furthermore to decrypt the catalytic species responsible in the rate-determining steps, we monitored the EPR spectra of **1**,**2** and **3** under catalytic conditions after performing control potential electrolysis at two different oxidizing

potentials (0.9 V and 1.2 V *vs.* Ag/AgCl). Note that, unlike non-catalytic conditions, where the oxidized species accumulate at anodic potential, the species in the catalytic cycle which are slow to react should accumulate under catalytic conditions. Indeed, as we have seen above, EPR provides a clear picture of the electronic states of the oxidized copper species together with the coordination scheme at the copper center. Persistent observation of a copper (II) signal was observed upon sequential oxidized samples under catalytic conditions (Fig. 7, Fig. S15).

No change in the β^2 (Cu^{2+}) value was observed for **1** (Table S3) in presence and absence of the substrate (TBAH), which suggests that base does not bind to the resting Cu(II) state which is further confirmed by the unaltered UV-VIS characteristics upon TBAH addition(Fig. S14A). A decrease in $\beta^2(Cu^{2+})$ was observed along with a change in $A_{II}(Cu^{2+})$ value (Table S3) upon oxidation at 0.9V in presence of TBAH with respect to the same in absence of TBAH which is an indication of the formation of a hydroxide bound Cu(II)-ligand monoradical species. The reduction in covalent charge donation due to the ligand oxidation is compensated by the hydroxide binding to the Cu leading to only a small decrease in β^2 (Cu^{2+}) value. There is no marked variation between the EPR signals observed after oxidation at 0.9 V (non-catalytic) and 1.2 V (catalytic) providing support that a Cu^{2+} (OH^-) ligand monoradical species is accumulated under catalytic steady-state and further oxidation of the hydroxide bound Cu^{2+}-ligand monoradical is the rate-determining step of the reaction. The total integrated spin calculated (Table S4, normalized with respect to the resting species in presence of TBAH) from the EPR signals (at 0.9V and 1.2V) was found to be unchanged and greater than 1 (Table S4) which further supports the accumulation of Cu^{2+}-ligand monoradical species which is a spin triplet as indicated by the spectroelectrochemical data under non-catalytic conditions. Note that, the presence of substantial amount of EPR silent diradical or Cu^{3+} species would have led to lower

spin integrations. Hence, these electronic snapshots, suggest that for **1**, after the first oxidation hydroxide binds to the Cu^{2+}-ligand monoradical, further oxidation of the monoradical species leads to the formation of the O-O bond via another attack of an OH^-. Note that the k_{cat} is 1^{st} order with respect to base (Fig. S3A) suggesting that the rate-determining oxidation of the Cu^{2+}-ligand monoradical is concerted with a base attached. This could either be deprotonation of the bound hydroxide to generate an oxyl radical or O-O bond formation via a nucleophilic attack of the hydroxide.

In the case of **2**, OH^- binds at the resting Cu (II) state as detected by the shift of β^2 (Cu^{2+}) value from 0.67 (in absence of TBAH) to 0.64 (in presence of TBAH) (Table S3). Hydroxide binding leads to an increase in the covalency of the resting Cu^{2+} species which reflects in the decrease in the β^2 (Cu^{2+}) value. The UV-VIS absorption data upon addition of TBAH shows a shift in the λ_{max} value from 427 nm to 454 nm (Fig. S14B) consistent with a change in the Cu^{2+} environment. The first oxidation at 0.9V forms a Cu^{2+}-ligand monoradical species (as indicated by an increase in β^2 (Cu^{2+}) value and an integrated total spin greater than 1) (Table S4). However, upon second oxidation at 1.2V, quenching of the radical signal was observed having an integrated spin less than 1 (normalized with respect to the hydroxide bound Cu^{2+} resting state) which indicate a) the accumulation of an EPR silent species under catalytic conditions and b) further oxidation of this species becomes the rate-determining step of the catalytic cycle. The diradical species is unlikely to be accumulated under catalytic condition (i.e. it is very reactive) as it would have not caused a reduction of total spin as the Cu^{2+}-diradical species is S=1/2 like the starting complex. Thus, for **2**, initially hydroxide binds to the resting Cu^{2+} state followed by two consecutive oxidations forming hydroxide bound Cu^{2+}-ligand diradical species and then an EPR silent species is formed whose forward reaction is the rate determining step of OER by **2**.

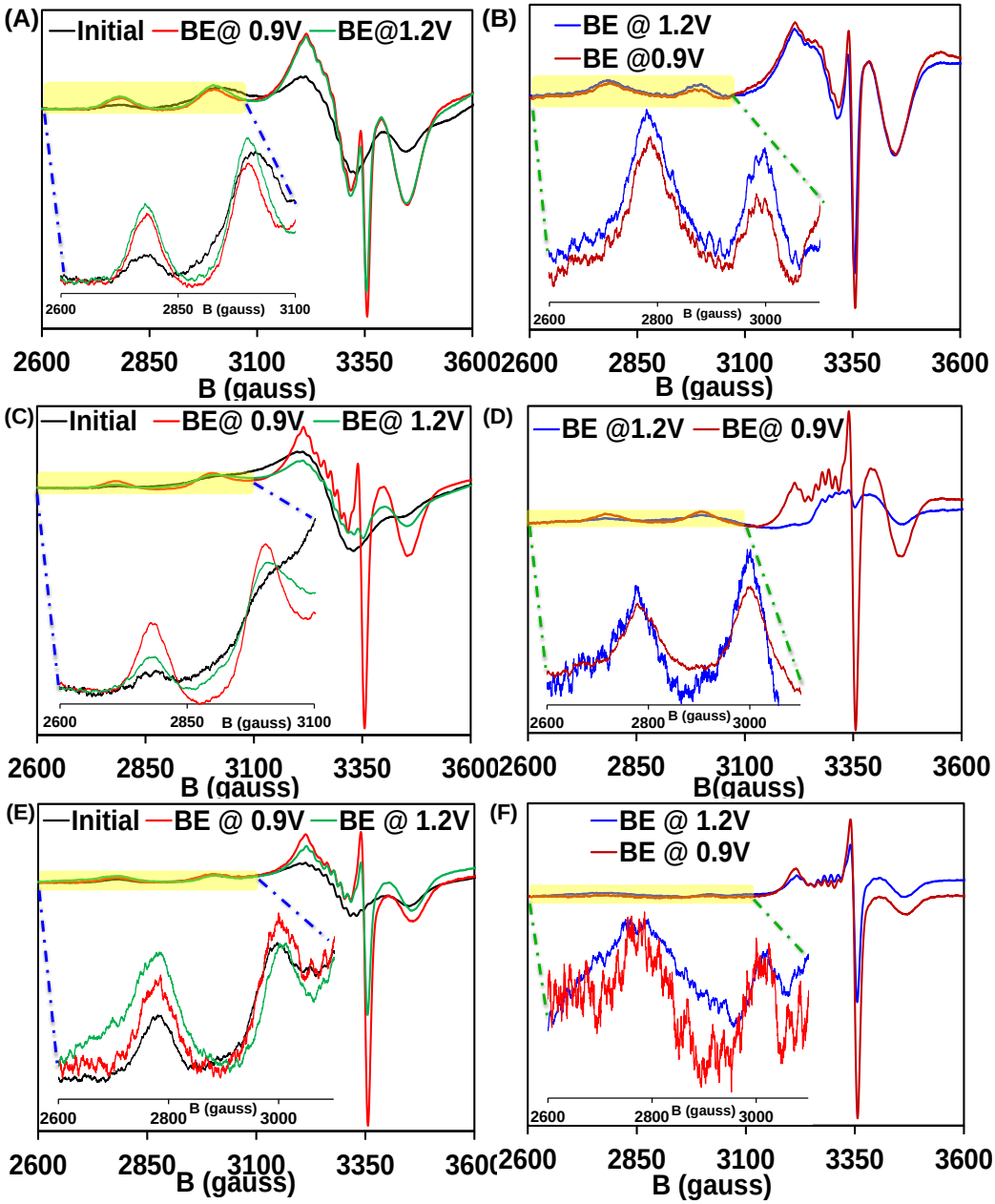

Figure 7: (A, C, and E) EPR spectra of **1**, **2**, and **3** in acetonitrile having 100 mM TBAP in presence of 7 mM TBAH (black-initial, red- after control potential electrolysis at 0.9V, green- after control potential electrolysis at 1.2V) respectively. (B, D, and F) EPR difference spectra (difference of the samples after respective oxidations from the initial in presence of 7 mM TBAH without bulk electrolysis) of the same.

Upon addition of TBAH to **3**, no change in β^2 value (Table S3) was seen along with unaltered UV-VIS characteristics (Fig. S14C) which tells us that base does not bind to the resting Cu^{2+} state. A Cu^{2+}-ligand monoradical (integrated spin greater than 1, Table S4) was seen in the EPR after the oxidation at 0.9V which bears the same EPR features (increase in β^2 value from the initial) as observed in the absence of substrate which indicates that hydroxide does not bind at the monoradical stage as well. Further oxidation at 1.2V accompanies with a slight decrease in integrated spin from 1 (Table S4), which indicates minor accumulation of an EPR silent species under catalytic steady-state similar to **2**. Thus, two successive electrochemical oxidations proceed for **3** forming Cu^{2+}-ligand diradical species whereupon hydroxide ion binds. The formation of O-O bond then completes after binding another hydroxide to the hydroxide bound Cu^{2+}-ligand diradical species since k_{cat} is 1^{st} order with respect to base (Fig. S11A).

(VI) FTIR spectroelectrochemistry under catalytic conditions:

When FTIR spectroelectrochemistry was done with **1** in the presence of 7 mM TBAH, the accumulation of the monoradical species with the amide vibrations at 1635 and 1714 cm^{-1} was observed under both non-catalytic (at 0.9 V) and catalytic conditions (at 1.2 V). (Fig. 8A, green and 8B) having the amide vibrations at 1635 and 1713 cm^{-1}. This is in accordance with the observation obtained from EPR that under catalytic steady state the monoradical species accumulates.

In the case of **3** in the presence of substrate, the accumulation of the monoradical species with the amide vibrations at 1661 and 1711 cm^{-1} was observed under non-catalytic conditions (at 0.9 V) which shift to 1661 and 1736 cm^{-1} (Fig. 8A, blue and 8D) when the bulk electrolysis was performed at 1.2 V (catalytic conditions). These values (at 1.2 V) are identical to those obtained in the absence of base and at 1.2 V (1663, and 1736 cm^{-1}) confirming it to be a Cu^{2+} bound

ligand based diradical species of **3**. Then in the next step, OH^- attack on this species, is likely to be the rate determining step of the OER by **3**.

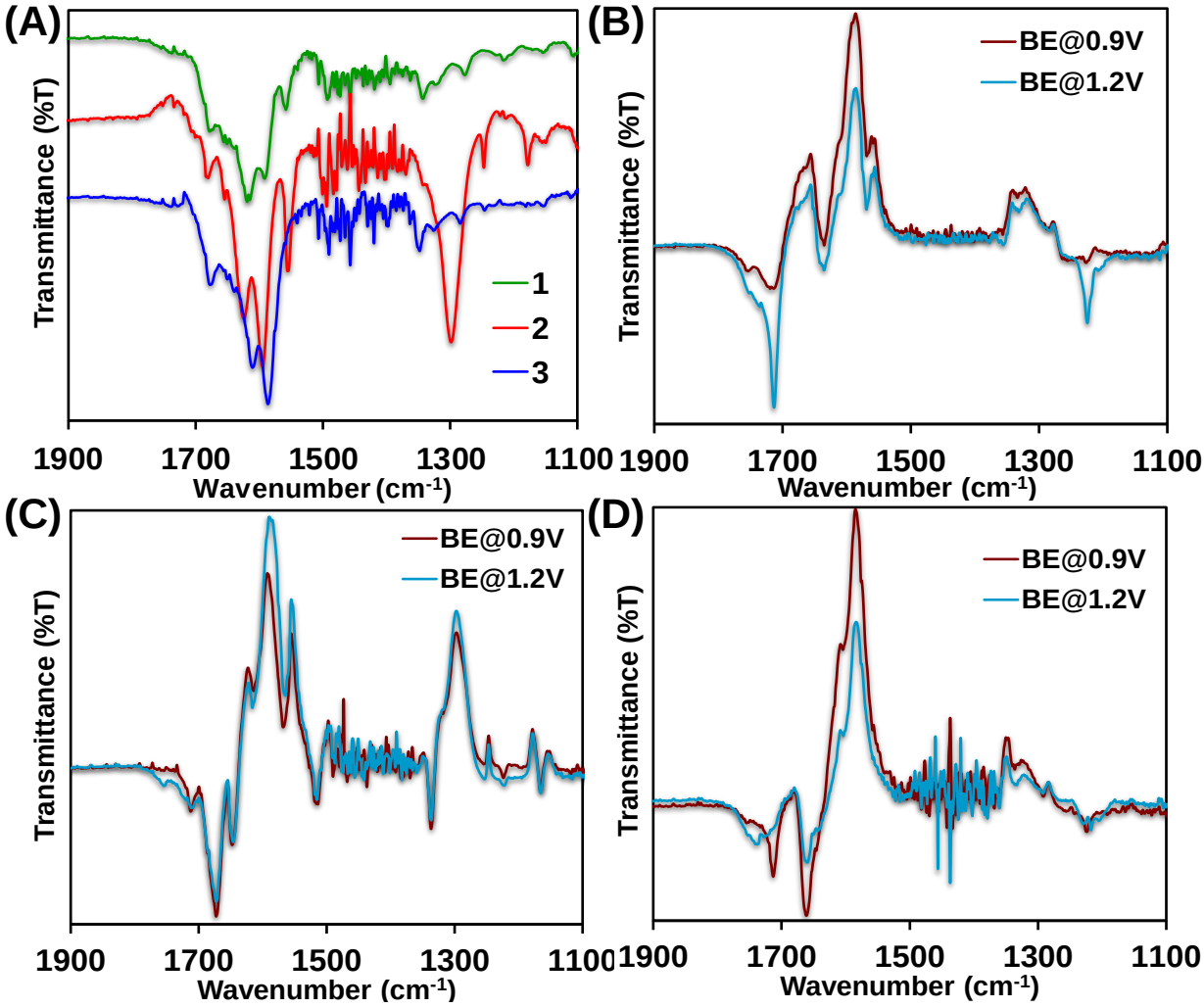

Figure 8: (A) FTIR spectra of the compounds (4 mM in acetonitrile having 100 mM TBAP electrolyte in presence of 7 mM TBAH) used in the present study, FTIR spectrochemical data (difference spectra- difference from the initial in acetonitrile having 7 mM TBAH without oxidation) of (B) **1**, (C) **2** and (D) **3** upon successive oxidations at 0.9V and 1.2V.

IR spectroelectrochemical spectra of **2** in the presence of TBAH under catalytic conditions (at 1.2 V) indicates the formation of mostly a Cu^{2+}-ligand monoradical species with the amide stretches at 1646 and 1672 cm^{-1} and a minor population of a Cu^{2+}-ligand diradical species having

amide vibrations at 1755 and 1712 cm^{-1}. The amide vibrations of the minor diradical species is slightly different from the Cu^{2+} diradical species characterized under non-catalytic conditions (1713, 1773 cm^{-1}) likely indicating an axial ligand bound to the Cu^{2+} center.

Thus, in the case of **2**, FTIR data indicates formation of a Cu^{2+}-monoradical species. However, the Cu^{2+}-monoradical species generated under non-catalytic conditions is EPR active and spin integration suggests that the spin on Cu^{2+} and ligand are either weakly ferromagnetically coupled or uncoupled. The spin integration of the EPR spectra under catalytic conditions indicates that the total spin is 0.86 when the starting complex spin integrates to 1.0. Thus, the EPR data obtained for the species accumulated under catalytic conditions suggest that this major monoradical species is an S=1/2 species and in addition to this there is a minor EPR silent diradical (FTIR) species. This EPR silent diradical species, may represent a diradical bound Cu^{3+}-OOH or a diradical bound Cu^{2+}-O_2^- species, or a mixture of both. A diradical bound Cu^{3+} species will require a potential much higher than that required to form the catalytically active Cu^{2+}-diradical state and can be eliminated. Similarly, a S=1/2 monoradical major species could be a monoradical bound to a Cu^{3+}-OOH or Cu^{2+}-O_2^-. To distinguish between these two species, we took the help of rR spectroscopy as the λ_{max} of the intermediate species is 450 nm.

(VII) rR spectroelectrochemistry of 2 under catalytic conditions:

The EPR data do not provide direct evidence for O-O bond formation. The O-O bond formation would lead to the formation of peroxide and superoxide species on its way to release O_2. While the Cu^{2+}-OOH species will have different ligand field than that of the Cu^{2+}-OH and would have resulted in a shift of the β^2 values and total spin would have been the same. Alternatively, a monoradical bound Cu^{2+}-O_2^- species or a Cu^{3+}-OOH could be EPR silent and may be observed in resonance Raman (rR). Compound **2** has Charge-transfer (CT) band near 450 nm and

corresponding rR experiments were done using λ_{ex} = 415 nm on frozen bulk electrolysis solutions at 77K. Complexes **1** and **3** have absorption between 350-380 nm which is not amenable to rR investigations without access to UV excitation wavelengths. Resonance Raman spectra of **2** in presence of TBAH after initial oxidation at 0.9 V reproducibly shows a vibration at 1180 cm^{-1} (additional independent data set in SI)(not present in rR of **2** after oxidation at 1.2V in the absence of TBAH, Fig. Sx) the intensity of which increases upon further oxidation at 1.2 V (Fig. S16B,C) and the value suggests that this could be the O-O vibration of a monoradical bound Cu^{2+}-O_2^- species (end-on).[62] The band near 1180 cm^{-1} shifts to 1127 cm^{-1} (Fig.7, Fig. 16B, C) upon ^{18}O labelling by using a solution of TBAH in H_2O^{18} which confirms the formation of a Cu^{2+}-O_2^- species during the course of the reaction.[63-64] Note that, the TBAH solution contains some unlabeled H_2O which is why there is residual intensity at 1180 cm^{-1} and minor intensity around 1165 cm^{-1} originating from $^{16}O_2^-$ and ^{16}O-^{18}-O mixed superoxide species produced. A monoradical bound Cu^{2+}-O_2^- species is likely to be EPR silent as the filled Cu^{2+} orbitals can mediate super exchange interaction (similar to the diradical anti-ferromagnetic coupling) between the O_2^- and ligand radical and could represent the EPR silent species formed under catalytic conditions in **2**. The bound O_2^- ligand is responsible for differences in both $A_{||}$ of the Cu^{2+} EPR and slight shifts in the diradical amide stretches relative to the diradical isolated under no-catalytic conditions. The high O-O vibration of this superoxide species (generally between 1100-1150 cm^{-1} for mononuclear Cu^{2+} complexes) indicates a strong Cu(II)-O bond. In an end-on Cu^{2+}-O_2^- species, superoxide donates electron to the Cu^{2+} from its π^* anti-bonding orbital which increases the Cu-O and O-O bond strength simultaneously. The presence of the oxidized ligand (ligand monoradical) makes Cu^{2+} more electron deficient as a result of which more electron donation takes place from the superoxide's π^* anti-bonding orbital to the Cu^{2+} shifting

the O-O bond vibration towards higher wavenumber. A strong Cu-O bond in the Cu^{2+}-O_2^- species would resist its hydrolysis deterring the formation of H_2O_2 (via disproportionation of O_2^-) which aligns well with minor H_2O_2 production and predominantly $4e^-/4H^+$ water oxidation selectively by **2** (as well as **1** and **3**).

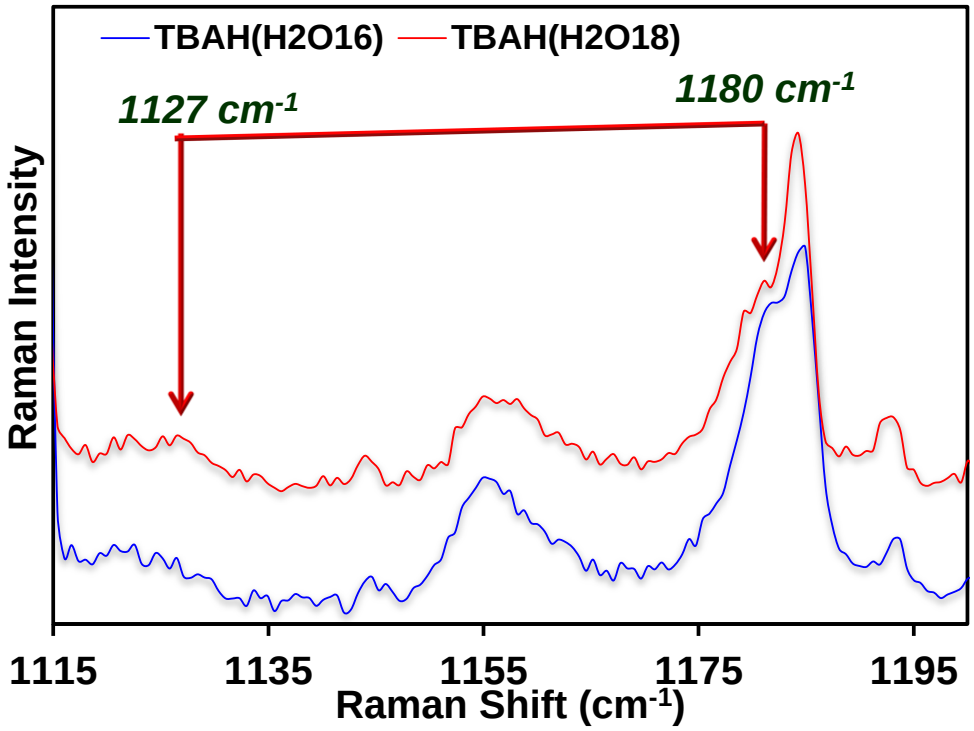

Figure 9: rR spectra at 77K of **2** having 100 mM TBAP in presence of 7 mM TBAH after control potential electrolysis at 1.2V (blue- TBAH in H_2O_{16} and red- TBAH in H_2O_{18}). The excitation wavelength is 415 nm.

Further oxidation of the monoradical Cu^{2+}-O_2^- species leads to the removal of another electron from the superoxide π* anti-bonding orbital leading to the formation of molecular O_2 and completes the catalytic cycle by bringing back the hydroxide bound Cu^{2+}-resting state as we observed previously that, hydroxide binds to the resting Cu^{2+}-state (in case of **2**) (Scheme 1).

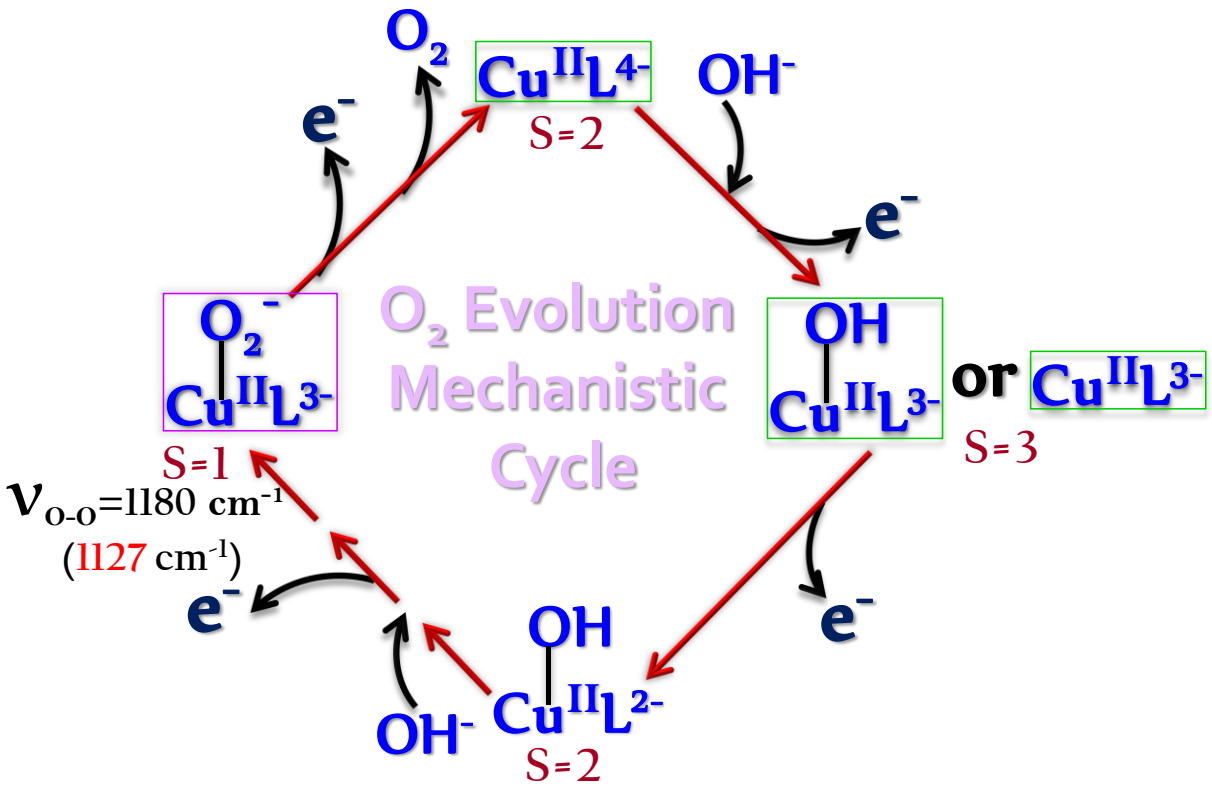

Scheme 1: Proposed mechanistic cycle for the evolution of molecular oxygen from water by Cu-complexes used in our study. The intermediates which are detected spectroscopically are written in rectangular box (green box- species identified by EPR, violet box- species identified by rR)

CONCLUSION

In conclusion, we have observed the electrocatalytic water oxidation with a family of copper (II) bis-oxamidate complex having a different electron-donating and withdrawing substituents in both organic and aqueous medium and the efficiency of the complexes towards electrocatalytic water oxidation reaction is dependent on the electron donating and withdrawing ability of the substituent present at the periphery. Heterogeneous electrochemistry revealed that compound **3** which have two electron-donating methyl substituent performs OER at 170 mV overpotential at pH 7. These catalysts are very selective towards water oxidation producing less than 1% H_2O_2 in both organic and aqueous medium. The mechanism of water oxidation in organic medium is

investigated using spectroelectrochemistry which suggests that both oxidation processes from the starting Cu^{2+} derivative are ligand centered under the operating conditions providing an alternate formulation of the active species responsible for the OER in the catalytic cycle. A Cu^{2+}-O_2^- species was identified as a reactive intermediate, further oxidation of which acts as the rds of the catalytic cycle. Strong Cu-O and O-O bonds in Cu^{2+}-O_2^-, minimizes the hydrolysis and thus avoids the formation of H_2O_2. Thus, it behaves as a key intermediate which is responsible for the selective oxidation of H_2O yielding 100% O_2.

ASSOCIATED CONTENT

Supporting Information.

Details of the experimental procedure, materials, additional electrochemical and spectroscopic data and crystallographic characterization are included in the ESI. †

AUTHOR INFORMATION

Corresponding Author

* Abhishek Dey: e-mail, icad@iacs.res.in.

* Ally Aukauloo: e-mail, ally.aukauloo@u-psud.fr

Funding Sources

This work was supported by the Department of Science and Technology Grant (SERB EMR-080063), the LABEX CHARMMMAT, and the French Infrastructure for integrated Structural Biology (FRISBI) ANR-10-INSB-05-01.

Notes

There are no conflicts to declare.

ACKNOWLEDGMENT

S.C. and A.G. are indebted to IACS IntPCS program and UGC-SRF respectively. We acknowledge Mr. Arnab Kumar Nath for helping us to collect the EPR data.

REFERENCES

1. Lewis, N. S.; Nocera, D. G., Powering the planet: Chemical challenges in solar energy utilization. *Proceedings of the National Academy of Sciences* **2006,** *103* (43), 15729.
2. Montoya, J. H.; Seitz, L. C.; Chakthranont, P.; Vojvodic, A.; Jaramillo, T. F.; Nørskov, J. K., Materials for solar fuels and chemicals. *Nature Materials* **2017,** *16* (1), 70-81.
3. Balzani, V.; Credi, A.; Venturi, M., Photochemical Conversion of Solar Energy. *ChemSusChem* **2008,** *1* (1- 2), 26-58.
4. Matheu, R.; Garrido-Barros, P.; Gil-Sepulcre, M.; Ertem, M. Z.; Sala, X.; Gimbert-Suriñach, C.; Llobet, A., The development of molecular water oxidation catalysts. *Nature Reviews Chemistry* **2019,** *3* (5), 331-341.
5. Simmons, T. R.; Berggren, G.; Bacchi, M.; Fontecave, M.; Artero, V., Mimicking hydrogenases: From biomimetics to artificial enzymes. *Coordination Chemistry Reviews* **2014,** *270-271*, 127-150.
6. Takeda, H.; Cometto, C.; Ishitani, O.; Robert, M., Electrons, Photons, Protons and Earth-Abundant Metal Complexes for Molecular Catalysis of CO2 Reduction. *ACS Catalysis* **2017,** *7* (1), 70-88.
7. Fukuzumi, S.; Lee, Y.-M.; Nam, W., Kinetics and mechanisms of catalytic water oxidation. *Dalton Transactions* **2019,** *48* (3), 779-798.
8. Cox, N.; Retegan, M.; Neese, F.; Pantazis, D. A.; Boussac, A.; Lubitz, W., Electronic structure of the oxygen-evolving complex in photosystem II prior to O-O bond formation. *Science* **2014,** *345* (6198), 804.
9. Lubitz, W.; Chrysina, M.; Cox, N., Water oxidation in photosystem II. *Photosynthesis Research* **2019,** *142* (1), 105-125.
10. Dau, H.; Grundmeier, A.; Loja, P.; Haumann, M., On the structure of the manganese complex of photosystem II: extended-range EXAFS data and specific atomic-resolution models for four S-states. *Philosophical Transactions of the Royal Society B: Biological Sciences* **2008,** *363* (1494), 1237-1244.
11. McEvoy, J. P.; Brudvig, G. W., Water-Splitting Chemistry of Photosystem II. *Chemical Reviews* **2006,** *106* (11), 4455-4483.
12. Yano, J.; Yachandra, V., Mn4Ca Cluster in Photosynthesis: Where and How Water is Oxidized to Dioxygen. *Chemical Reviews* **2014,** *114* (8), 4175-4205.
13. Suga, M.; Akita, F.; Sugahara, M.; Kubo, M.; Nakajima, Y.; Nakane, T.; Yamashita, K.; Umena, Y.; Nakabayashi, M.; Yamane, T.; Nakano, T.; Suzuki, M.; Masuda, T.; Inoue, S.; Kimura, T.; Nomura, T.; Yonekura, S.; Yu, L.-J.; Sakamoto, T.; Motomura, T.; Chen, J.-H.;

Kato, Y.; Noguchi, T.; Tono, K.; Joti, Y.; Kameshima, T.; Hatsui, T.; Nango, E.; Tanaka, R.; Naitow, H.; Matsuura, Y.; Yamashita, A.; Yamamoto, M.; Nureki, O.; Yabashi, M.; Ishikawa, T.; Iwata, S.; Shen, J.-R., Light-induced structural changes and the site of O=O bond formation in PSII caught by XFEL. *Nature* **2017,** *543* (7643), 131-135.
14. Askerka, M.; Brudvig, G. W.; Batista, V. S., The O2-Evolving Complex of Photosystem II: Recent Insights from Quantum Mechanics/Molecular Mechanics (QM/MM), Extended X-ray Absorption Fine Structure (EXAFS), and Femtosecond X-ray Crystallography Data. *Accounts of Chemical Research* **2017,** *50* (1), 41-48.
15. Umena, Y.; Kawakami, K.; Shen, J.-R.; Kamiya, N., Crystal structure of oxygen-evolving photosystem II at a resolution of 1.9 Å. *Nature* **2011,** *473* (7345), 55-60.
16. Zhang, W.; Lai, W.; Cao, R., Energy-Related Small Molecule Activation Reactions: Oxygen Reduction and Hydrogen and Oxygen Evolution Reactions Catalyzed by Porphyrin- and Corrole-Based Systems. *Chemical Reviews* **2017,** *117* (4), 3717-3797.
17. Kanady, J. S.; Tsui, E. Y.; Day, M. W.; Agapie, T., A Synthetic Model of the Mn_3Ca Subsite of the Oxygen-Evolving Complex in Photosystem II. *Science* **2011,** *333* (6043), 733.
18. Zhang, C.; Chen, C.; Dong, H.; Shen, J.-R.; Dau, H.; Zhao, J., A synthetic Mn₄Ca-cluster mimicking the oxygen-evolving center of photosynthesis. *Science* **2015,** *348* (6235), 690.
19. Cox, N.; Pantazis, D. A.; Neese, F.; Lubitz, W., Biological Water Oxidation. *Accounts of Chemical Research* **2013,** *46* (7), 1588-1596.
20. Kärkäs, M. D.; Verho, O.; Johnston, E. V.; Åkermark, B., Artificial Photosynthesis: Molecular Systems for Catalytic Water Oxidation. *Chemical Reviews* **2014,** *114* (24), 11863-12001.
21. Codolá. Z, L. F. J., Costas.M. , Catalytic Water Oxidation: Water Oxidation to O2 Mediated by 3d Transition Metal Complexes. In *Non- Noble Metal Catalysis*, Wiley Online Library: 2020; pp 425-451.
22. Gersten, S. W.; Samuels, G. J.; Meyer, T. J., Catalytic oxidation of water by an oxo-bridged ruthenium dimer. *Journal of the American Chemical Society* **1982,** *104* (14), 4029-4030.
23. Chronister, C. W.; Binstead, R. A.; Ni, J.; Meyer, T. J., Mechanism of Water Oxidation Catalyzed by the μ-Oxo Dimer [(bpy)2(OH2)RuIIIORuIII(OH2)(bpy)2]4+. *Inorganic Chemistry* **1997,** *36* (18), 3814-3815.
24. Hull, J. F.; Balcells, D.; Blakemore, J. D.; Incarvito, C. D.; Eisenstein, O.; Brudvig, G. W.; Crabtree, R. H., Highly Active and Robust Cp* Iridium Complexes for Catalytic Water Oxidation. *Journal of the American Chemical Society* **2009,** *131* (25), 8730-8731.
25. Joya, K. S.; Subbaiyan, N. K.; D'Souza, F.; de Groot, H. J. M., Surface-Immobilized Single-Site Iridium Complexes for Electrocatalytic Water Splitting. *Angewandte Chemie International Edition* **2012,** *51* (38), 9601-9605.
26. Matheu, R.; Ertem, M. Z.; Gimbert-Suriñach, C.; Sala, X.; Llobet, A., Seven Coordinated Molecular Ruthenium–Water Oxidation Catalysts: A Coordination Chemistry Journey. *Chemical Reviews* **2019,** *119* (6), 3453-3471.
27. Vereshchuk, N.; Matheu, R.; Benet-Buchholz, J.; Pipelier, M.; Lebreton, J.; Dubreuil, D.; Tessier, A.; Gimbert-Suriñach, C.; Ertem, M. Z.; Llobet, A., Second Coordination Sphere Effects in an Evolved Ru Complex Based on Highly Adaptable Ligand Results in Rapid Water Oxidation Catalysis. *Journal of the American Chemical Society* **2020,** *142* (11), 5068-5077.

28. Panda, C.; Debgupta, J.; Díaz Díaz, D.; Singh, K. K.; Sen Gupta, S.; Dhar, B. B., Homogeneous Photochemical Water Oxidation by Biuret-Modified Fe-TAML: Evidence of FeV(O) Intermediate. *Journal of the American Chemical Society* **2014,** *136* (35), 12273-12282.
29. Karlsson, E. A.; Lee, B.-L.; Åkermark, T.; Johnston, E. V.; Kärkäs, M. D.; Sun, J.; Hansson, Ö.; Bäckvall, J.-E.; Åkermark, B., Photosensitized Water Oxidation by Use of a Bioinspired Manganese Catalyst. *Angewandte Chemie International Edition* **2011,** *50* (49), 11715-11718.
30. Wang, H.-Y.; Mijangos, E.; Ott, S.; Thapper, A., Water Oxidation Catalyzed by a Dinuclear Cobalt–Polypyridine Complex. *Angewandte Chemie International Edition* **2014,** *53* (52), 14499-14502.
31. Schöfberger, W.; Faschinger, F.; Chattopadhyay, S.; Bhakta, S.; Mondal, B.; Elemans, J. A. A. W.; Müllegger, S.; Tebi, S.; Koch, R.; Klappenberger, F.; Paszkiewicz, M.; Barth, J. V.; Rauls, E.; Aldahhak, H.; Schmidt, W. G.; Dey, A., A Bifunctional Electrocatalyst for Oxygen Evolution and Oxygen Reduction Reactions in Water. *Angewandte Chemie International Edition* **2016,** *55* (7), 2350-2355.
32. Brudvig, G. W., Catalysing water oxidation using nature's metal. *Nature Catalysis* **2018,** *1* (1), 10-11.
33. Hong, D.; Mandal, S.; Yamada, Y.; Lee, Y.-M.; Nam, W.; Llobet, A.; Fukuzumi, S., Water Oxidation Catalysis with Nonheme Iron Complexes under Acidic and Basic Conditions: Homogeneous or Heterogeneous? *Inorganic Chemistry* **2013,** *52* (16), 9522-9531.
34. Liu, T.; Zhang, B.; Sun, L., Iron-Based Molecular Water Oxidation Catalysts: Abundant, Cheap, and Promising. *Chemistry – An Asian Journal* **2019,** *14* (1), 31-43.
35. Barnett, S. M.; Goldberg, K. I.; Mayer, J. M., A soluble copper–bipyridine water-oxidation electrocatalyst. *Nature Chemistry* **2012,** *4* (6), 498-502.
36. Zhang, M.-T.; Chen, Z.; Kang, P.; Meyer, T. J., Electrocatalytic Water Oxidation with a Copper(II) Polypeptide Complex. *Journal of the American Chemical Society* **2013,** *135* (6), 2048-2051.
37. Zhang, X.; Li, Y.-Y.; Jiang, J.; Zhang, R.; Liao, R.-Z.; Wang, M., A Dinuclear Copper Complex Featuring a Flexible Linker as Water Oxidation Catalyst with an Activity Far Superior to Its Mononuclear Counterpart. *Inorganic Chemistry* **2020,** *59* (8), 5424-5432.
38. Shen, J.; Zhang, X.; Cheng, M.; Jiang, J.; Wang, M., Electrochemical Water Oxidation Catalyzed by N4-Coordinate Copper Complexes with Different Backbones: Insight into the Structure-Activity Relationship of Copper Catalysts. *ChemCatChem* **2020,** *12* (5), 1302-1306.
39. Su, X.-J.; Zheng, C.; Hu, Q.-Q.; Du, H.-Y.; Liao, R.-Z.; Zhang, M.-T., Bimetallic cooperative effect on O–O bond formation: copper polypyridyl complexes as water oxidation catalyst. *Dalton Transactions* **2018,** *47* (26), 8670-8675.
40. Kafentzi, M.-C.; Papadakis, R.; Gennarini, F.; Kochem, A.; Iranzo, O.; Le Mest, Y.; Le Poul, N.; Tron, T.; Faure, B.; Simaan, A. J.; Réglier, M., Electrochemical Water Oxidation and Stereoselective Oxygen Atom Transfer Mediated by a Copper Complex. *Chemistry – A European Journal* **2018,** *24* (20), 5213-5224.
41. Nestke, S.; Ronge, E.; Siewert, I., Electrochemical water oxidation using a copper complex. *Dalton Transactions* **2018,** *47* (31), 10737-10741.
42. Stott, L. A.; Prosser, K. E.; Berdichevsky, E. K.; Walsby, C. J.; Warren, J. J., Lowering water oxidation overpotentials using the ionisable imidazole of copper(2-(2′-pyridyl)imidazole). *Chemical Communications* **2017,** *53* (3), 651-654.

43. Gerlach, D. L.; Bhagan, S.; Cruce, A. A.; Burks, D. B.; Nieto, I.; Truong, H. T.; Kelley, S. P.; Herbst-Gervasoni, C. J.; Jernigan, K. L.; Bowman, M. K.; Pan, S.; Zeller, M.; Papish, E. T., Studies of the Pathways Open to Copper Water Oxidation Catalysts Containing Proximal Hydroxy Groups During Basic Electrocatalysis. *Inorganic Chemistry* **2014,** *53* (24), 12689-12698.
44. Serrano-Plana, J.; Garcia-Bosch, I.; Company, A.; Costas, M., Structural and Reactivity Models for Copper Oxygenases: Cooperative Effects and Novel Reactivities. *Accounts of Chemical Research* **2015,** *48* (8), 2397-2406.
45. Kuilya, H.; Alam, N.; Sarma, D.; Choudhury, D.; Kalita, A., Ligand assisted electrocatalytic water oxidation by a copper(ii) complex in neutral phosphate buffer. *Chemical Communications* **2019,** *55* (38), 5483-5486.
46. Garrido-Barros, P.; Funes-Ardoiz, I.; Drouet, S.; Benet-Buchholz, J.; Maseras, F.; Llobet, A., Redox Non-innocent Ligand Controls Water Oxidation Overpotential in a New Family of Mononuclear Cu-Based Efficient Catalysts. *Journal of the American Chemical Society* **2015,** *137* (21), 6758-6761.
47. Garrido-Barros, P.; Gimbert-Suriñach, C.; Moonshiram, D.; Picón, A.; Monge, P.; Batista, V. S.; Llobet, A., Electronic π-Delocalization Boosts Catalytic Water Oxidation by Cu(II) Molecular Catalysts Heterogenized on Graphene Sheets. *Journal of the American Chemical Society* **2017,** *139* (37), 12907-12910.
48. Ruiz, R.; Surville-Barland, C.; Aukauloo, A.; Anxolabehere-Mallart, E.; Journaux, Y.; Cano, J.; Carmen Muñoz, M., Stabilization of copper(III) complexes by disubstituted oxamides and related ligands. *Journal of the Chemical Society, Dalton Transactions* **1997,** (5), 745-752.
49. Anson, F. C.; Collins, T. J.; Richmond, T. G.; Santarsiero, B. D.; Toth, J. E.; Treco, B. G. R. T., Highly stabilized copper(III) complexes. *Journal of the American Chemical Society* **1987,** *109* (10), 2974-2979.
50. Ottenwaelder, X.; Ruiz-García, R.; Blondin, G.; Carasco, R.; Cano, J.; Lexa, D.; Journaux, Y.; Aukauloo, A., From metal to ligand electroactivity in nickel(ii) oxamato complexes. *Chemical Communications* **2004,** (5), 504-505.
51. Gordon-Wylie, S. W.; Claus, B. L.; Horwitz, C. P.; Leychkis, Y.; Workman, J. M.; Marzec, A. J.; Clark, G. R.; Rickard, C. E. F.; Conklin, B. J.; Sellers, S.; Yee, G. T.; Collins, T. J., New Magnetically Coupled Bimetallic Complexes as Potential Building Blocks for Magnetic Materials. *Chemistry – A European Journal* **1998,** *4* (11), 2173-2181.
52. de Bellefeuille, D.; Orio, M.; Barra, A.-L.; Aukauloo, A.; Journaux, Y.; Philouze, C.; Ottenwaelder, X.; Thomas, F., Redox Noninnocence of the Bridge in Copper(II) Salophen and Bis(oxamato) Complexes. *Inorganic Chemistry* **2015,** *54* (18), 9013-9026.
53. Kanso, H.; Clarke, R. M.; Kochem, A.; Arora, H.; Philouze, C.; Jarjayes, O.; Storr, T.; Thomas, F., Effect of Distortions on the Geometric and Electronic Structures of One-Electron Oxidized Vanadium(IV), Copper(II), and Cobalt(II)/(III) Salen Complexes. *Inorganic Chemistry* **2020,** *59* (7), 5133-5148.
54. Pratt, R. C.; Stack, T. D. P., Intramolecular Charge Transfer and Biomimetic Reaction Kinetics in Galactose Oxidase Model Complexes. *Journal of the American Chemical Society* **2003,** *125* (29), 8716-8717.
55. Pratt, R. C.; Lyons, C. T.; Wasinger, E. C.; Stack, T. D. P., Electrochemical and Spectroscopic Effects of Mixed Substituents in Bis(phenolate)–Copper(II) Galactose Oxidase Model Complexes. *Journal of the American Chemical Society* **2012,** *134* (17), 7367-7377.

56. Asami, K.; Tsukidate, K.; Iwatsuki, S.; Tani, F.; Karasawa, S.; Chiang, L.; Storr, T.; Thomas, F.; Shimazaki, Y., New Insights into the Electronic Structure and Reactivity of One-Electron Oxidized Copper(II)-(Disalicylidene)diamine Complexes. *Inorganic Chemistry* **2012,** *51* (22), 12450-12461.
57. Chaudhuri, P.; Verani, C. N.; Bill, E.; Bothe, E.; Weyhermüller, T.; Wieghardt, K., Electronic Structure of Bis(o-iminobenzosemiquinonato)metal Complexes (Cu, Ni, Pd). The Art of Establishing Physical Oxidation States in Transition-Metal Complexes Containing Radical Ligands. *Journal of the American Chemical Society* **2001,** *123* (10), 2213-2223.
58. Verma, P.; Pratt, R. C.; Storr, T.; Wasinger, E. C.; Stack, T. D. P., Sulfanyl stabilization of copper-bonded phenoxyls in model complexes and galactose oxidase. *Proceedings of the National Academy of Sciences* **2011,** *108* (46), 18600.
59. Zink, J. I.; Drago, R. S., Interpretation of electron spin resonance parameters for transition metal complexes. *Journal of the American Chemical Society* **1972,** *94* (13), 4550-4554.
60. Seal, M.; Dey, S. G., Active-Site Environment of Copper-Bound Human Amylin Relevant to Type 2 Diabetes. *Inorganic Chemistry* **2018,** *57* (1), 129-138.
61. Ghosh, C.; Dey, S. G., Ligand-Field and Ligand-Binding Analysis of the Active Site of Copper-Bound Aβ Associated with Alzheimer's Disease. *Inorganic Chemistry* **2013,** *52* (3), 1318-1327.
62. Elwell, C. E.; Gagnon, N. L.; Neisen, B. D.; Dhar, D.; Spaeth, A. D.; Yee, G. M.; Tolman, W. B., Copper–Oxygen Complexes Revisited: Structures, Spectroscopy, and Reactivity. *Chemical Reviews* **2017,** *117* (3), 2059-2107.
63. Donoghue, P. J.; Gupta, A. K.; Boyce, D. W.; Cramer, C. J.; Tolman, W. B., An Anionic, Tetragonal Copper(II) Superoxide Complex. *Journal of the American Chemical Society* **2010,** *132* (45), 15869-15871.
64. Woertink, J. S.; Tian, L.; Maiti, D.; Lucas, H. R.; Himes, R. A.; Karlin, K. D.; Neese, F.; Würtele, C.; Holthausen, M. C.; Bill, E.; Sundermeyer, J.; Schindler, S.; Solomon, E. I., Spectroscopic and Computational Studies of an End-on Bound Superoxo-Cu(II) Complex: Geometric and Electronic Factors That Determine the Ground State. *Inorganic Chemistry* **2010,** *49* (20), 9450-9459.